Rock Mech. Rock Engng. (2005) 38 (5), 345–372
DOI 10.1007/s00603-005-0059-2

Rock Mechanics and Rock Engineering
Printed in Austria

Practical Estimate of Deformations and Stress Relief Factors for Deep Tunnels Supported by Shotcrete

By

A. Graziani, D. Boldini, and **R. Ribacchi**

Department of Structural and Geotechnical Engineering,
University of Rome "La Sapienza", Italy

Received March 16, 2004; accepted March 17, 2005
Published online June 2, 2005

Summary

Even though ground-support interaction in the vicinity of the tunnel face is a typical 3D problem, tunnel support design is usually based on simplified plane strain models, which are strongly dependent on the assumed degree of ground stress relief at the time of lining installation. The paper focuses on tunnels supported by shotcrete close to the face, where the interaction between the loading process and progressive hardening of the green shotcrete makes the problem time-dependent. A constitutive law characterized by the time-dependent stiffness and strength of the shotcrete is employed herein. The results of an extensive parametric study based on 3D axisymmetric models are presented in the form of non-dimensional design charts, which can provide guidance to a preliminary evaluation of convergences and support loadings.

Moreover a strategy is proposed to enhance the capability of simplified design methods (2D models, Convergence-Confinement Method). This consists in a "guided estimate" of stress relief factors, which again is based on the results of 3D time-dependent analyses. Finally, by way of example, the proposed method is applied to two well-documented case-histories.

Keywords: Deep tunnels, shotcrete, design methods.

1. Introduction

Nowadays shotcrete is considered to be a fundamental support element for tunnels driven by conventional excavation methods in poor rock masses. The shotcrete layer is generally applied near the tunnel face so as to reduce the yielding of the surrounding ground and limit short-term deformations. Thanks to the time-increasing stiffness and strength, and to the creep properties of green shotcrete, the stress-strain conditions within the lining can satisfy safety requirements even in poor quality rock masses, where large deformations are likely to occur before the ground reaches a new equilibrium.

Shotcrete finds application both in sequential and full-face excavation. Full-face excavation, often associated with face reinforcement by means of fiber-glass dowels where face instability is anticipated, has recently spread throughout Europe, especially in France and Italy. Even if this construction technique is widely adopted nowadays (Lunardi, 2000; Hoek, 2001), the available design methods are not completely satisfactory.

Tunnel design is generally based on over-simplified schematizations of the real construction process, with local failures during construction, if any, being overcome by relying heavily on the experience of the contractors and consultants involved in the project. The application of numerical modeling to the prediction of tunnel behavior is still a challenging task because of the following issues:

- The modeling of excavation advance and support installation near the face is essentially a 3D problem; nevertheless plane strain 2D models are still more popular because 3D modeling is time-consuming and requires more skill and experience in analyzing the results;
- Ground conditions along the route of the tunnel can only be approximately predicted before the beginning of the excavation; moreover, the overall behavior of the tunnel is significantly affected by many details of the construction technology (excavation phases, quality of the shotcrete and accuracy of its application) in addition to the mechanical parameters of the ground and support system;
- The state of stress within the shotcrete layer is markedly influenced by the progressive hardening of the green concrete, which occurs simultaneously with load increase driven by face advance; other time-dependencies may stem from a decrease in the long-term strength of the disturbed rock mass around the excavation, as well as from the viscous behavior of the shotcrete and of the rock.

Therefore a compromise needs to be found between rough design methods and detailed numerical modeling in order to obtain a predictive tool effectively suited to tunneling practice. The Convergence-Confinement Method (CCM) (AFTES, 1983), based on the simplified assumption of a circular tunnel in a hydrostatic stress field, represents a classical answer to this requirement. Nevertheless a careful analysis has shown (Wong and Kaiser, 1991; Bernaud and Rousset, 1996) that loads are usually underestimated by the conventional CCM procedure.

This observation has prompted a refinement of the CCM known as New Implicit Method (NIM) (Nguyen Minh and Corbetta, 1991; Bernaud and Rousset, 1992).

More recently Oreste (2003) has further improved the conventional CCM by applying a numerical procedure to obtain a support reaction curve which takes the time-dependent stiffness of the shotcrete into account.

Indeed, a more general criticism can be addressed to all plane models, including 2D FEM models: the effect of excavation advance can only be represented by some artifices and therefore ground-support interaction is only roughly evaluated especially when shotcrete is applied after each excavation round, because of the strong interaction between the time-dependent hardening of the shotcrete and the simultaneous increase in loading induced by the next face advance.

An approach that is deemed to be more direct and easier to apply than that of the NIM is therefore presented herein. The full-face excavation of quasi-circular deep

tunnels has been simulated step-by-step by 3D-axisymmetric FEM models, in which the stiffness and strength properties of the shotcrete lining are continuously updated (Cosciotti et al., 2001). The results have been conveniently utilized to calibrate the stress relief factor at the tunnel wall whereby the face effect is simulated in simplified CCM or in 2D-FEM calculations.

2. Conventional Design Methods for Deep Tunnels

Usually, the 3D problem of tunnel excavation is analyzed by an equivalent plane strain problem in which the influence of the face is simply simulated by applying a support pressure p_i at the tunnel wall, as initially proposed in the CCM (Lombardi, 1973; Panet and Guellec, 1974).

Following the hypothesis of a circular tunnel having radius a and hydrostatic stress field σ_o assumed in the CCM, the applied pressure must be uniform within the tunnel section and should be determined in such a way that the convergence of the plane section equals that of the real tunnel in 3D conditions.

The fictitious internal pressure p_i can therefore be expressed as a decreasing function of distance x from the face

$$p_i(x) = [1 - \lambda(x)]\sigma_o, \tag{1}$$

where λ represents a stress release factor, i.e., the fraction of the initial stress to be removed at a given distance x: $\lambda = 0$ applies to the ground far ahead of the tunnel face, while $\lambda = 1$ applies to the unsupported tunnel section at a great distance from the face.

The ground-lining interaction is evaluated in the CCM by considering separately the behavior of the ground and of the lining represented respectively by the *convergence curve*, and by the *confinement curve*.

The former represents the relationship between the internal pressure p_i and the radial displacement of the tunnel wall u; for an elastic medium it reads:

$$u = \frac{1+\nu}{E}(\sigma_o - p_i)a. \tag{2}$$

For an elasto-plastic medium a number of analytical solutions are available, for instance Ribacchi and Riccioni (1977), Brown et al. (1983) and Carranza-Torres (2003).

The *confinement curve* represents the relationship between the pressure q applied on the extrados of the lining and the radial displacement:

$$q = K_s \frac{(u - u_0)}{a}, \quad \text{with } K_s = E_s \frac{e}{a} \tag{3}$$

where K_s is the stiffness of the shotcrete annulus (thickness e) and u_0 is the radial displacement of the tunnel wall at the time of lining installation.

The equilibrium conditions of the supported tunnel are represented by the intersection of the *convergence curve* with the *confinement curve* (Fig. 1). The main uncertainty of the method is the evaluation of the radial displacement u_0, or, similarly, of the fictitious internal pressure p_i at the time of lining installation.

In the conventional CCM, the wall displacement at the time of lining installation, u_0, is easily obtained by one of the available equations (Panet and Guenot, 1982;

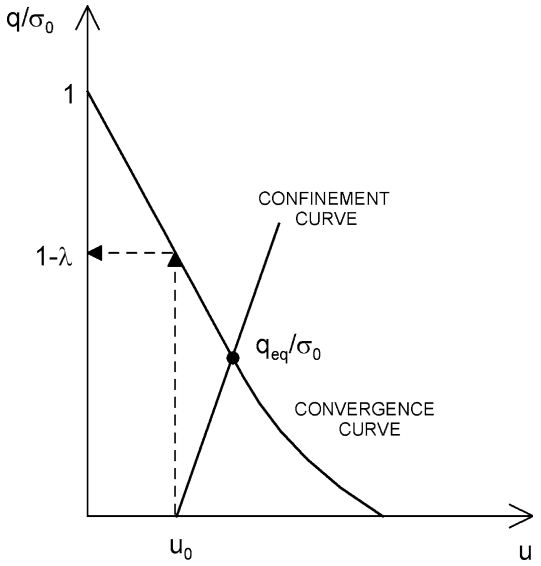

Fig. 1. Schema of the Convergence-Confinement method (CCM)

Corbetta et al., 1991) which relate the wall displacement of an unsupported tunnel to the face distance. For example the well-known expression of Panet and Guenot (1982) is:

$$u(x) = u_f + (u_\infty - u_f) \cdot \left[1 - \left(\frac{0.84 \cdot R_p}{x + 0.84 \cdot R_p}\right)^2\right], \tag{4}$$

where u_f is the radial displacement of the tunnel wall at the face and u_∞ is the displacement at a great distance from the face (R_p is the plastic radius). For an elastic medium the asymptotic displacement u_∞ can be obtained from Eq. (2), assuming $p_i = 0$; while u_f is equal to $0.27 \cdot u_\infty$. The last relationship approximately holds also for an elasto-plastic medium, if u_∞ is evaluated accordingly.

However, 3D numerical models show that tunnel convergence at the time of lining installation at a given distance x depends on the stiffness of the lining itself (Kielbassa and Duddeck, 1991; Bernaud and Rousset, 1992). In other words, lining installation modifies tunnel wall convergence even in the unsupported length between lining and face: the higher the stiffness of the lining, the lower the tunnel convergence. Therefore, the conventional approach implies an overestimation of the wall displacement u_0 at the time of lining installation, which in turn leads to an underestimation of the final load on the lining.

Bernaud and Rousset (1992) elaborated a simplified method (NIM) to obtain more reliable predictions of support loadings on the basis of the results provided by 3D models. They substantially redefined relationship (4), giving a new expression of wall displacement as a function of face distance, in which the influence of the stiffness of the lining, represented as a linear elastic structure, is taken into account.

However, the NIM cannot be directly applied to the problem at hand because it does not take into account the effect of the time-dependent hardening of the shotcrete.

A common shortcut in practice is simply to assume a lower value for the shotcrete elastic modulus, representative of the average behavior of green concrete. On the basis of numerical modeling, Pöttler (1990) has suggested a modulus of 7 GPa, almost independent of specific ground properties and construction rate; however, some different values have also been applied, e.g., a modulus of only 2 GPa for the Kielder Experimental Tunnel (Stille et al., 1989).

In the approach proposed herein, still based on 3D model results, preference has been attached to working on the evaluation of the stress relief factors λ at the time of lining placement, because of the following reasons:

- wide popularity of the λ-method in engineering practice (Vogt et al., 1998; Hoek, 2001);
- possibility of combining various effects (lining stiffness, progressive hardening, excavation phases) in a single fictitious parameter;
- ease of generalizing the results to non-axisymmetric conditions, e.g. 2D FEM models, for non-circular tunnels, non-hydrostatic in situ stresses, etc.

3. Description of the Problem

The axisymmetric problem of a circular tunnel excavated through a medium subjected to isotropic and homogeneous in situ stress σ_o is considered.

The construction process consists of alternating phases of excavation advance and shotcrete application. After each excavation round, characterized by a specified length l, a layer of shotcrete of thickness e is applied to the tunnel wall up to the face. These cycles of excavation and shotcrete application are repeated continuously and steady-state conditions are rapidly reached within a distance of only a few rounds from the face.

3.1 Constitutive Laws of Ground Mass and Shotcrete

The ground mass is modeled by means of a linear elastic (Young's modulus E and Poisson's ratio ν) perfectly plastic law, characterized by a Mohr-Coulomb strength criterion (cohesion c, friction angle φ and dilation angle ψ).

An elasto-plastic constitutive law characterized by time-dependent stiffness and strength has been used for shotcrete. Increase in the elastic modulus E_s and in the uniaxial compressive strength σ_s as a function of time has been expressed by the following empirical relationships proposed by Chang (1994), while the Poisson ratio ν_s is constant

$$E_s(t)/E_{s,28} = c_1 \exp(c_2/t^{c_3}) \tag{5}$$

$$\sigma_s(t)/\sigma_{s,28} = d_1 \exp(d_2/t^{d_3}), \tag{6}$$

where c_1, c_2, c_3, d_1, d_2 and d_3 are material constants equal to 1.062, −0.446, 0.6, 1.105, −0.743 and 0.7, if time t is expressed in days. Young's modulus and the uniaxial compressive strength of shotcrete at 28 days are given by $E_{s,28}$ and $\sigma_{s,28}$,

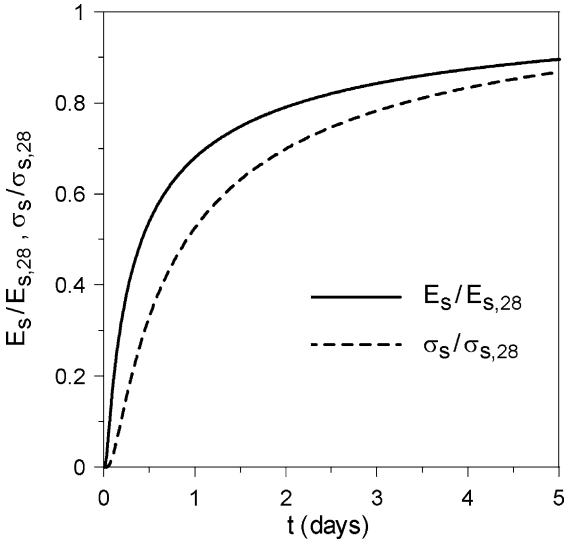

Fig. 2. Functions describing the time-dependence of Young's modulus E_s and uniaxial compressive strength σ_s of the shotcrete

respectively. The time evolution of the scaled modulus $E_s/E_{s,28}$ and uniaxial compressive strength $\sigma_s/\sigma_{s,28}$ are illustrated in Fig. 2.

Relationships (5) and (6) have been obtained by fitting data from all kinds of shotcrete including dry- and wet-mixed, accelerated and steel-fiber reinforced shotcrete. The scatter of experimental data is reported to be generally low for fresh shotcrete (up to 1–2 days old) while it increases for older shotcrete (Sezaki et al., 1989; Chang, 1994).

Moreover, the hardening process strongly reduces the ductile behavior of freshly applied shotcrete, which up to 0.5–1 day typically exhibits an ideal-plastic behavior with failure strain as high as 3–4%. Indeed, it will be shown in the following that the rock-support interaction is mainly affected by the mechanical behavior of freshly applied shotcrete.

3.2 Non-dimensional Parameters

The problem of ground-lining interaction is governed by a large number of parameters which account for the mechanical behavior of the ground, the mechanical behavior of the lining and the construction process.

Nevertheless, by performing a dimensional analysis and by examining the differential equations of the elasto-plastic boundary value problem, the number of significant parameters, and thus the computational effort, can be reduced.

As a starting point, let's consider the case of a tunnel supported by an internal pressure equal to a given value q. Anagnostou and Kovari (1993) have shown that the displacements are proportional to $1/E$ even for an opening in yielding ground, and that the influence of cohesion is statically equivalent to an increase $c/tan\varphi$ in the support

pressure and in the isotropic in situ stress. Therefore the following relationship holds for the radial displacement u of the tunnel wall

$$\frac{uE}{a(\sigma_o + c/tan\varphi)} = f\left(\frac{q + c/tan\varphi}{\sigma_o + c/tan\varphi}, \nu, \varphi, \psi\right). \tag{7}$$

When an effective interaction problem is addressed, in which the support pressure is supplied by a linear elastic lining of stiffness K_s, the first non-dimensional parameter on the right side of Eq. (7) must be broken down, since q is no longer an a priori known value. Equation (7) now becomes

$$\frac{uE}{a\sigma_o} = f\left(\frac{c}{\sigma_o}, \frac{K_s}{E}, \frac{l}{2a}, \nu, \varphi, \psi\right), \tag{8}$$

where a new variable l is moreover introduced to represent the tunnel length excavated and supported at each step.

In the case of shotcrete lining, Eq. (8) must be further modified to account for the time-dependent behavior of the material. A full description of the process of shotcrete hardening would require the definition of both the final characteristic values and the time-evolution laws of stiffness and strength. For the sake of simplicity, it is assumed that the evolution laws are defined once and for all by Eqs. (5) and (6), while $E_{s,28}$ and $\sigma_{s,28}$ represent variable parameters. In this case, two new non-dimensional parameters should be included, $K_{s,28}/E$ and $q_{s,28}/\sigma_o$, to represent respectively the relative stiffness and yield load (pressure) of the shotcrete annulus at 28 days

$$\frac{K_{s,28}}{E} = \frac{E_{s,28}}{E} \cdot \frac{e}{a} \qquad \frac{q_{s,28}}{\sigma_o} = \frac{\sigma_{s,28}}{\sigma_o} \cdot \frac{e}{a}. \tag{9}$$

Moreover the interrelationship between the loading process and hardening of the shotcrete is accounted for by the following non-dimensional parameter

$$\frac{2a}{28\mathrm{v}} \quad (\mathrm{v\ expressed\ as}\ length/day) \tag{10}$$

which represents the ratio of two characteristic times: $2a/\mathrm{v}$, the time required to excavate a tunnel length equal to one tunnel diameter, and 28 days, the time necessary for the shotcrete to reach its conventional final stiffness and strength.

The left side of Eq. (8), multiplied by $(1 + \nu)$, is equal to the ratio between the actual displacement u and the displacement of the unsupported elastic tunnel u^{*el}, given by (2). The final form of the functional relationship (8) is therefore

$$\frac{u}{u^{*el}} = f\left(\frac{c}{\sigma_o}, \frac{K_{s,28}}{E}, \frac{q_{s,28}}{\sigma_o}, \frac{2a}{28\mathrm{v}}, \frac{l}{2a}, \nu, \varphi, \psi\right). \tag{11}$$

4. Numerical Model

4.1 Finite Difference Mesh and Calculation Steps

The numerical analyses have been performed with the Finite Difference code FLAC (Itasca, 2000). Figure 3 shows the extension and boundary conditions of the axisymmetric calculation grid, which consists of about 9500 nodes.

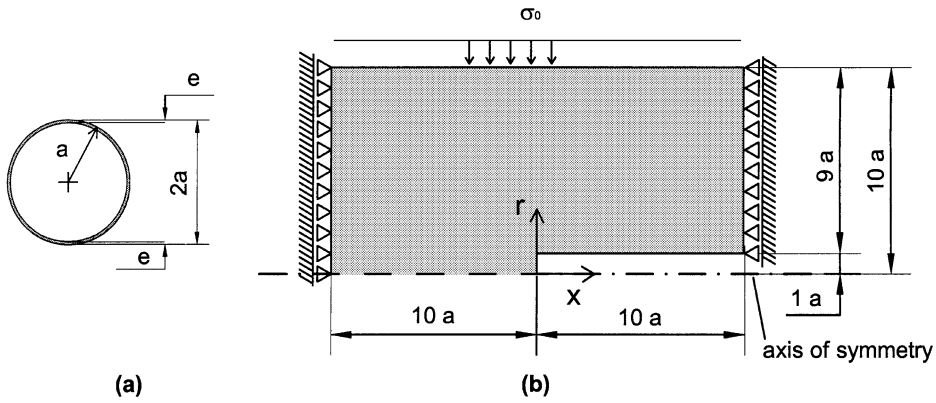

Fig. 3. Geometric properties of the numerical model

The coordinate axes x and r coincide respectively with the tunnel axis and the radial direction; the origin corresponds to the final position reached by the tunnel face after simulating a total excavation advance equal to 10a. Such length is sufficient to reach steady state conditions and to eliminate almost any influence of the outer boundary conditions on the near-face state of stress and strain.

Near the tunnel wall the mesh is refined in order to provide a better approximation of the higher stress gradients (Fig. 4a). The initial state of stress is introduced as an isotropic stress σ_o within the elements of the grid and by applying tractions at the outer radial boundary. The excavation process has been simulated by applying a step-wise procedure as illustrated in Fig. 4b. At each excavation step (length l) a set of ground elements are changed into null elements; shotcrete application is simulated in the next step by changing a strip of null elements into elements with shotcrete properties. The

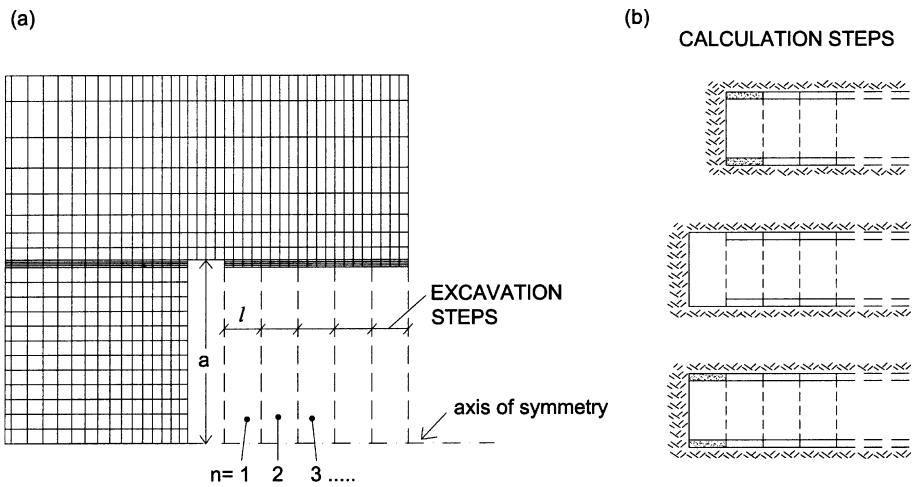

Fig. 4. Detail of the finite difference grid near the tunnel face (**a**) and sketch of the calculation steps (**b**)

Table 1. Shotcrete age at first loading for different values of the tunnel excavation rate and length of the excavation step

Tunnel excavation rate	Shotcrete age at first loading	
v (m/day)	$l = 1$ m	$l = 2$ m
2	6 hours	12 hours
4	3 hours	6 hours

excavation and the shotcrete installation steps are repeated iteratively until the final face position ($x = 0$) is reached.

The time assigned to the excavation step and to the shotcrete application step is the same: e.g., for a tunnel advance rate of 2 m/day and rounds of length $l = 1$ m, 1 meter of tunnel is completed in 12 h, half of which is assigned to excavation and half to shotcrete application.

As shown later, ground-shotcrete interaction in tunneling is mainly influenced by the age of the shotcrete at the first loading near the tunnel face. Shotcrete age at first loading depends on the tunnel excavation rate and on the length of the excavation step. For ease of reference, shotcrete age at first loading for a typical range of values of v and l is reported in Table 1.

4.2 Parametric Analysis

The effect of the time-dependent stiffness of shotcrete has been extensively analyzed while the time-dependent yield strength has been considered only in a subset of cases. The properties assumed for the shotcrete annulus are representative of typical support systems utilized in current practice, in a wide range of ground conditions. Table 2 summarizes all the values assumed for the single variables and the corresponding non-dimensional parameters.

Table 2. Ground and support properties assumed in the numerical analyses and associated non-dimensional parameters

Single parameters	Non-dimensional parameters
$\sigma_o = 1.5$ MPa	$\frac{c}{\sigma_o} = 0.044,\ 0.087,\ 0.175,\ 0.350,\ 0.700$
$E = 90,\ 900,\ 9000$ MPa	$\nu = 0.25$
$c = 0.066,\ 0.131,\ 0.262,\ 0.525,\ 1.050$ MPa	$\varphi = 20°,\ 35°$
$\nu = 0.25$	$\psi = 0°,\ 10°$
$\varphi = 20°,\ 35°$	$\frac{l}{2a} = 0.1,\ 0.2$
$\psi = 0°,\ 10°$	$\frac{K_{s,28}}{E} = 10.7,\ 1.07,\ 0.107$
$a = 5$ m	$\frac{q_{s,28}}{\sigma_o} = 0.16,\ 0.80$
$e = 0.2$ m	$\frac{2a}{28\text{v}} = \infty,\ 0.18,\ 0.09,\ 0.045,\ 0$
$l = 1,\ 2$ m	
$E_{s,28} = 24$ GPa	
$\nu = 0.3$	
$\sigma_{s,28} = 6,\ 30$ MPa	
$\text{v}_s = 0,\ 2,\ 4,\ 8,\ \infty$ m/d	

4.3 Typical Results

Before undertaking a comprehensive analysis of the whole set of numerical results, it is worthwhile describing the typical features of tunnel behavior, as predicted by a step-by-step simulation.

The typical pattern of radial stress in the ground surrounding the tunnel face (Fig. 5) shows the development of a bearing arch in the ground spanning from the face to the nearest end of the lining, after each excavation round. As a consequence, the state of stress within each shotcrete segment is far from being uniform, especially if an elastic behavior is assumed for the shotcrete, as in the case of Fig. 6, where the axial forces, N_θ and N_x, and the bending moments, M_θ and M_x, acting within the

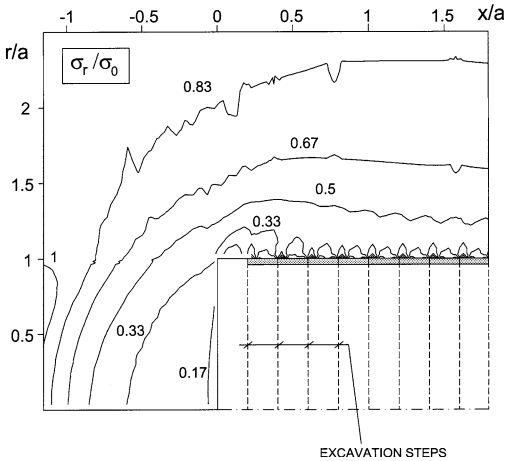

Fig. 5. Typical pattern of radial stresses in the ground near the tunnel face ($K_{s,28}/E = 10.7$, $c/\sigma_o = 0.087$, $\varphi = 20°$, $\psi = 0°$, v = 2 m/d, $l = 1$ m)

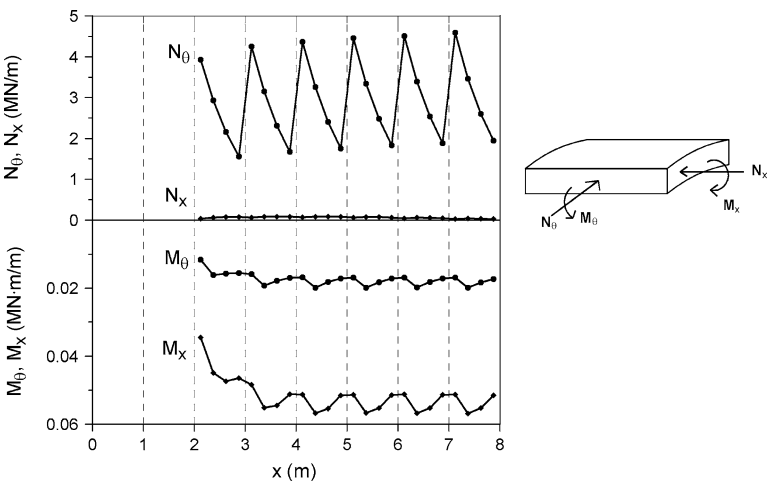

Fig. 6. Axial forces, N_θ and N_x, and bending moments, M_θ and M_x within the shotcrete segments ($K_{s,28}/E = 10.7$, $c/\sigma_o = 0.087$, $\varphi = 20°$, $\psi = 0°$, v = 2 m/d, $l = 1$ m)

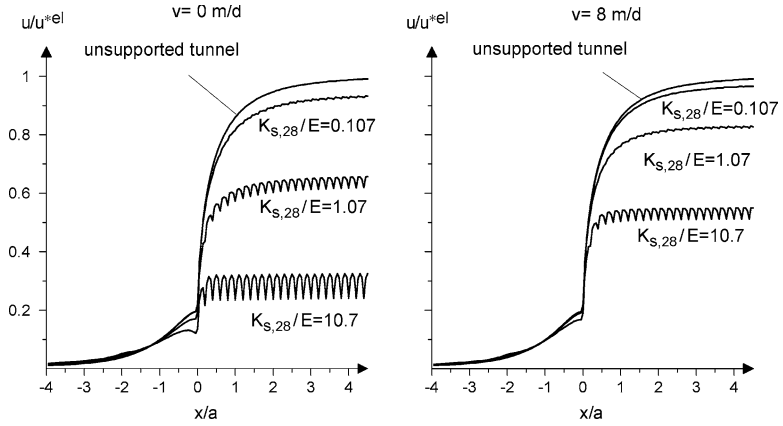

Fig. 7. Normalized radial displacement profile of the tunnel wall for different values of $K_{s,28}/E$ and v (elastic ground, elastic lining, $l = 1$ m)

shotcrete segments closest to the face, are represented (θ and x indicate respectively the circumferential and longitudinal directions).

The longitudinal force N_x is more than one order smaller than the circumferential force N_θ. The x-profile of N_θ is characterized by a saw-toothed shape, where each saw-tooth corresponds to one excavation step. Within each segment, N_θ reaches the maximum value at the point closest to the face, which is about 1.5 times greater than the average value $N_{\theta m}$ within the segment.

A saw-toothed shape characterizes also the convergence profile of the tunnel wall: Figure 7 shows the normalized displacement of the tunnel wall u/u^{*el} as a function of the face distance x, for different values of relative stiffness $K_{s,28}/E$ and excavation rate v.

The stiffer the shotcrete annulus with respect to the ground, the lower the normalized displacement u/u^{*el}, i.e. the same lining is more effective in reducing tunnel convergence in a softer ground, as recognized intuitively.

Figure 7 also shows that by increasing the excavation rate v, the convergence increases. In fact for a given face distance x, the stiffness of the shotcrete lining is lower when the excavation proceeds faster, resulting in a reduced support action. A further effect of a faster excavation rate is a smoothing down of the stress-strain field, which assumes a more uniform profile along each shotcrete segment.

5. Design Charts

The results of the parametric analyses can be used to obtain approximate guidelines on the design of shotcrete-supported tunnels. A set of design charts have been compiled by focusing on a minimum number of parameters relevant to a preliminary design stage:

- the average load q within a shotcrete annulus of length l, calculated as $N_{\theta m}/a$;
- the radial displacements u of the tunnel wall, averaged within the length l;
- the radial displacement u_{shot} undergone by the shotcrete annulus, again averaged within the length l.

The aforementioned parameters refer to ''equilibrium'' conditions, i.e., to the stationary state reached at a section of the tunnel when the distance from the face is such that

any further advance has a negligible influence on the current stress-strain conditions. Such a distance is mostly less than twice the tunnel diameter (Fig. 7).

The reasons underlying the option of considering only the ''average'' behavior of a tunnel segment are twofold:

– from a practical point of view, the many uncertainties concerning the actual tunnel behavior (see Section 1) and the small size of the pull-length l in the current tunneling practice ($l = 1$–2 m), make the use of point-values a less sensible choice;
– from a theoretical point a view, it is easier to make comparisons with other conventional calculation methods, such as the CCM and 2D plane models.

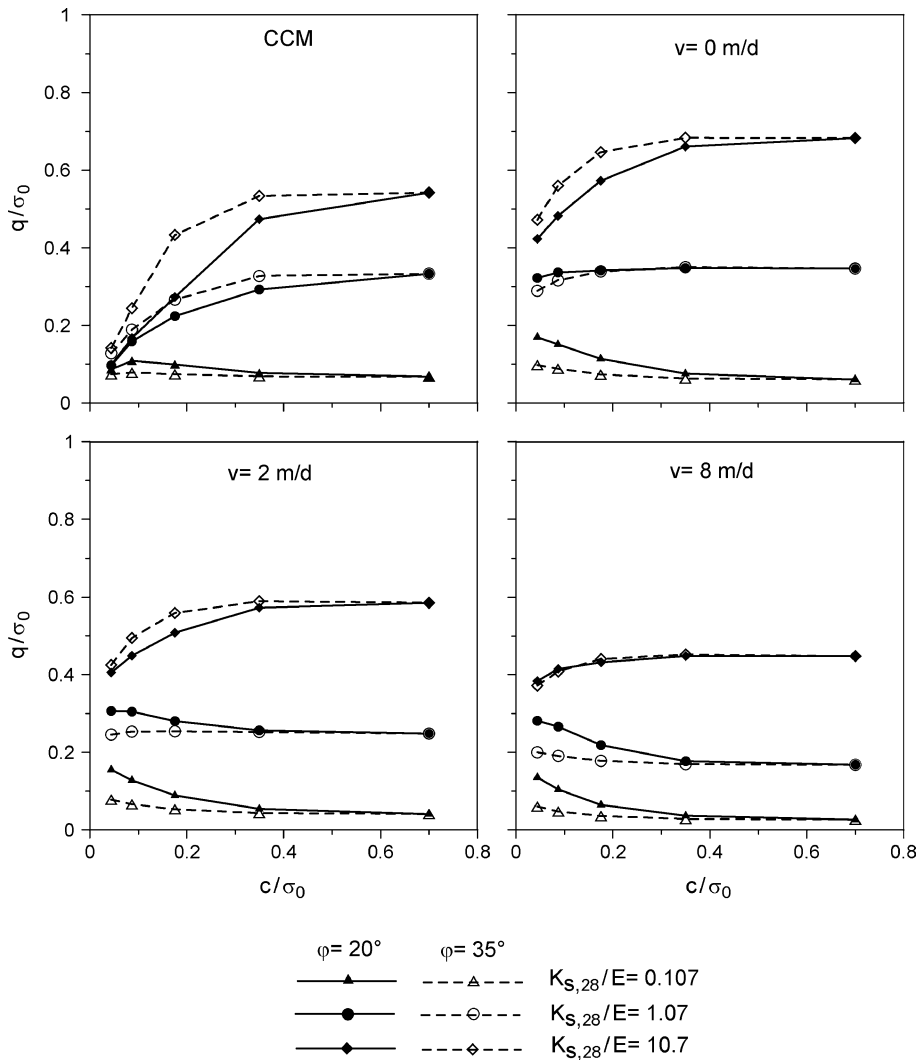

Fig. 8. Equilibrium load q on the shotcrete annulus (elastic lining, $\psi = 0°$, $l = 1$ m)

The results are presented in non-dimensional form, as a function of the significant ground-support parameters identified in Section 3.2.

First the basic case of an elastic lining in an elasto-plastic ground is illustrated (Figs. 8–10), followed by a specific analysis of the dilatancy effect (Fig. 11); next the impact of the plastic yielding of the shotcrete (Figs. 12–14), and finally the influence of the pull-length l is investigated (Fig. 15). Only for the basic case of elastic shotcrete behavior has the effect of a variable excavation rate v been extensively analyzed; for the other cases only the typical value of $v = 2\,m/d$ is discussed.

Figure 8 shows the normalized load q/σ_o obtained for a range of values of the non-dimensional parameters K_s/E, c/σ_o, φ and different advance rates v. In agreement with the already observed behavior in a purely elastic ground (Fig. 7), the relative stiffness K_s/E is the factor with the strongest influence on the support effect.

The relative increase in the load with K_s/E is maximum in the limit case of a constant stiffness lining ($v = 0$) and less important as the advance rate increases.

The effect of the ground strength parameters, c/σ_o and φ, is less intuitive. Its trend is quite different for different values of relative stiffness. For a high value of K_s/E, an increase in strength (c/σ_o or φ) produces an increase in load, while the opposite behavior is observed for a low value of K_s/E.

The unforeseen results of less severe loadings in poorer ground conditions can be tentatively explained by comparing the two CCM solutions (elastic and elasto-plastic) reported in Fig. 9. The decrease in the loading in the plastic case is caused by the increased convergence u_0 before the installation of the lining, which overshadows the negative effect of the flattening of the convergence curve in the plastic range.

The CCM results (Fig. 8) are in agreement with the numerical results obtained for high strength ground and low-stiffness support if the effect of the excavation rate is disregarded ($v = 0$). On the contrary, the CCM drastically underestimates the values of

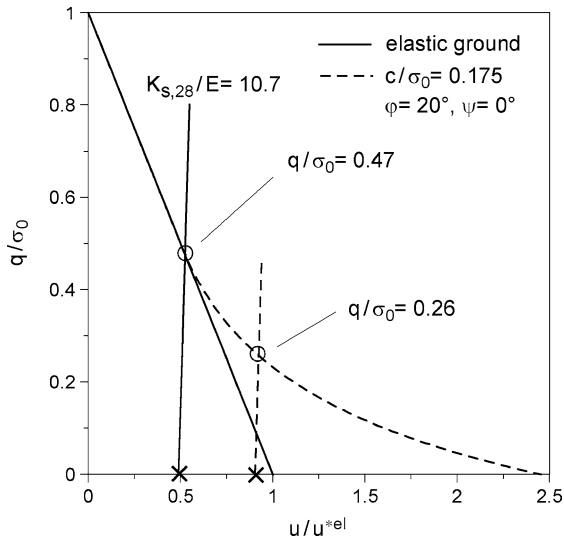

Fig. 9. CCM results for two typical ground conditions

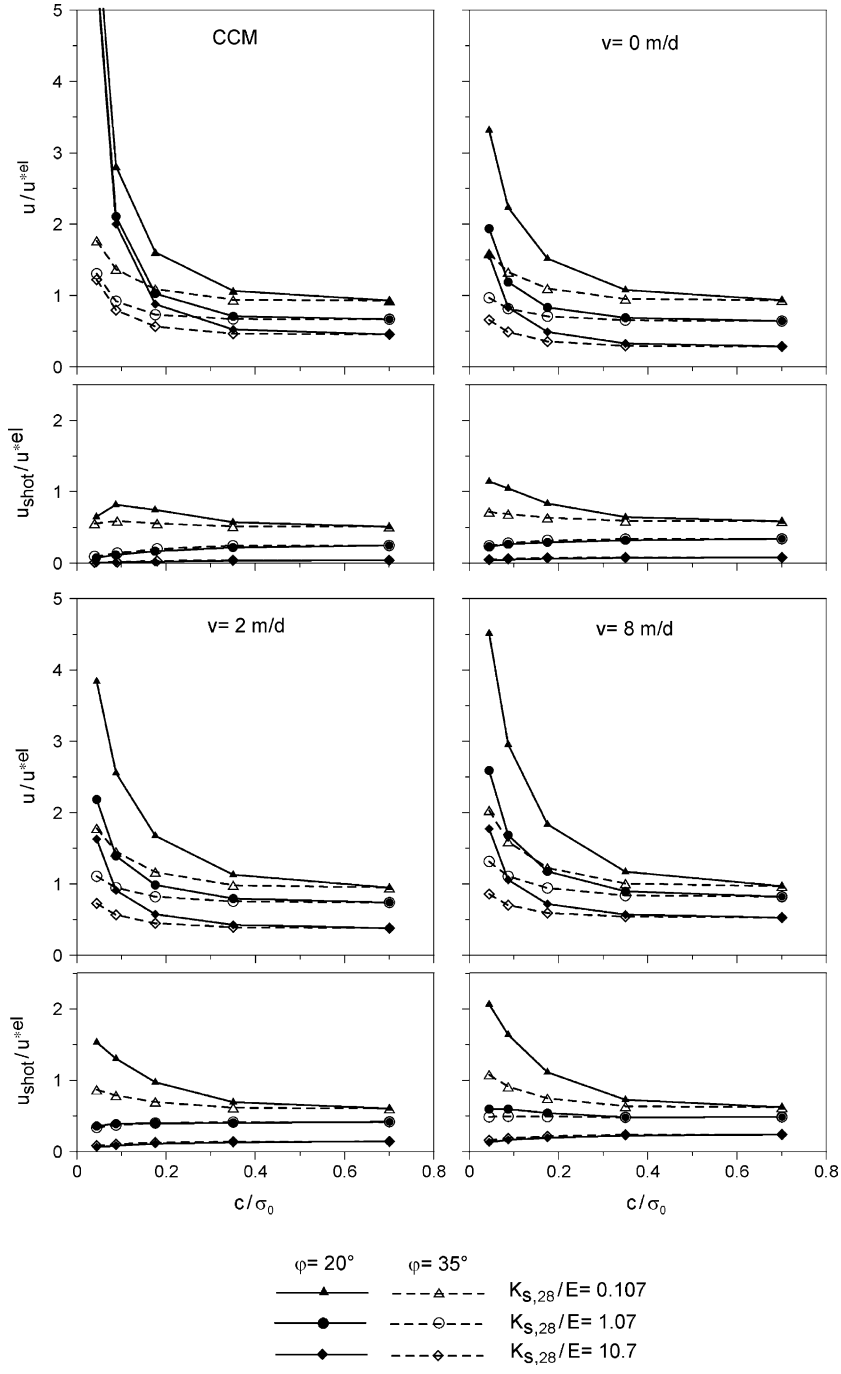

Fig. 10. Radial displacement of the tunnel wall u and of the shotcrete lining u_{shot} (elastic lining, $\psi = 0°$, $l = 1\,\text{m}$)

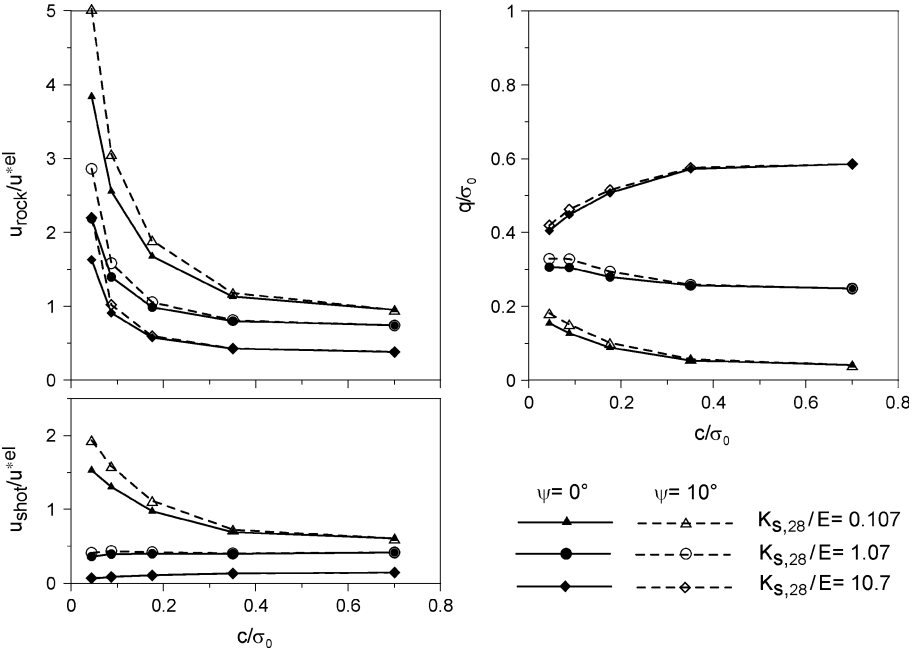

Fig. 11. Influence of ground dilatancy on the equilibrium load q, tunnel wall displacement u and shotcrete lining displacement u_{shot} (elastic lining, $\varphi = 20°$, $l = 1\,\text{m}$, $\text{v} = 2\,\text{m/d}$)

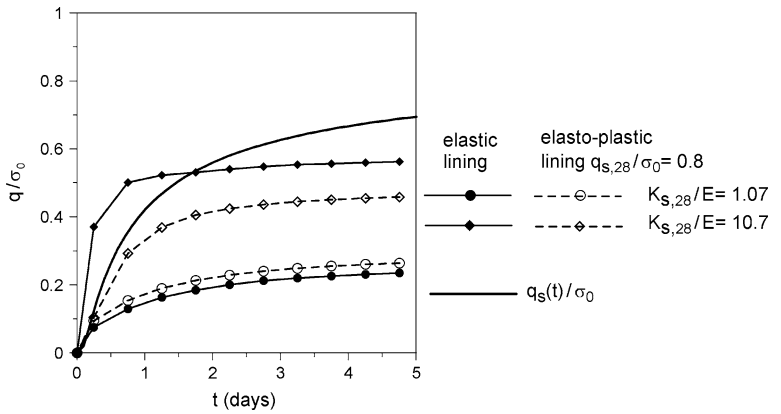

Fig. 12. Time-development of the lining load q for elastic and elasto-plastic shotcrete behavior ($\text{v} = 2\,\text{m/d}$, $c/\sigma_{\text{o}} = 0.35$, $\varphi = 20°$, $\psi = 0°$, $l = 1\,\text{m}$)

q/σ_{o} for low-strength ground conditions, giving values of the loads up to four times lower in the case of high relative stiffness.

The response of the tunnel in terms of total displacements of the wall (Fig. 10) exhibits a simpler trend, with monotonically increasing displacements as the strength of the ground (c and φ) decreases; the higher scaled displacements u/u^{*el} occur at lower relative stiffness conditions, as expected.

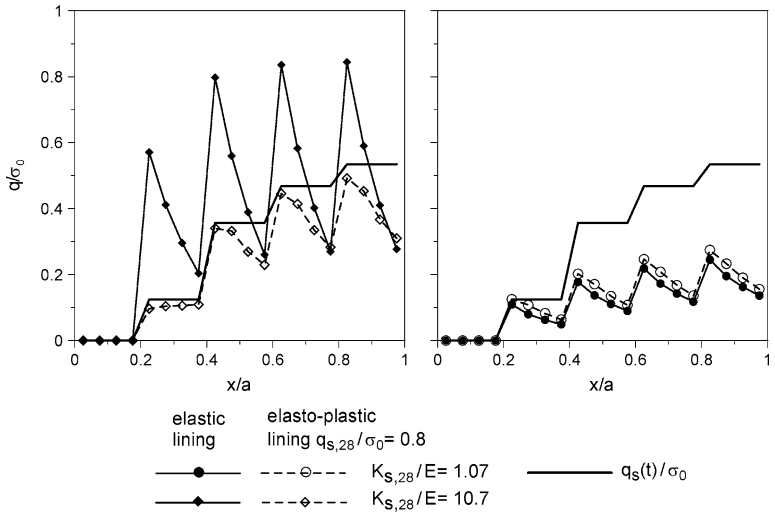

Fig. 13. Load distribution on the lining for elastic and elasto-plastic shotcrete behavior ($v = 2\,m/d$, $c/\sigma_o = 0.35$, $\varphi = 20°$, $\psi = 0°$, $l = 1\,m$)

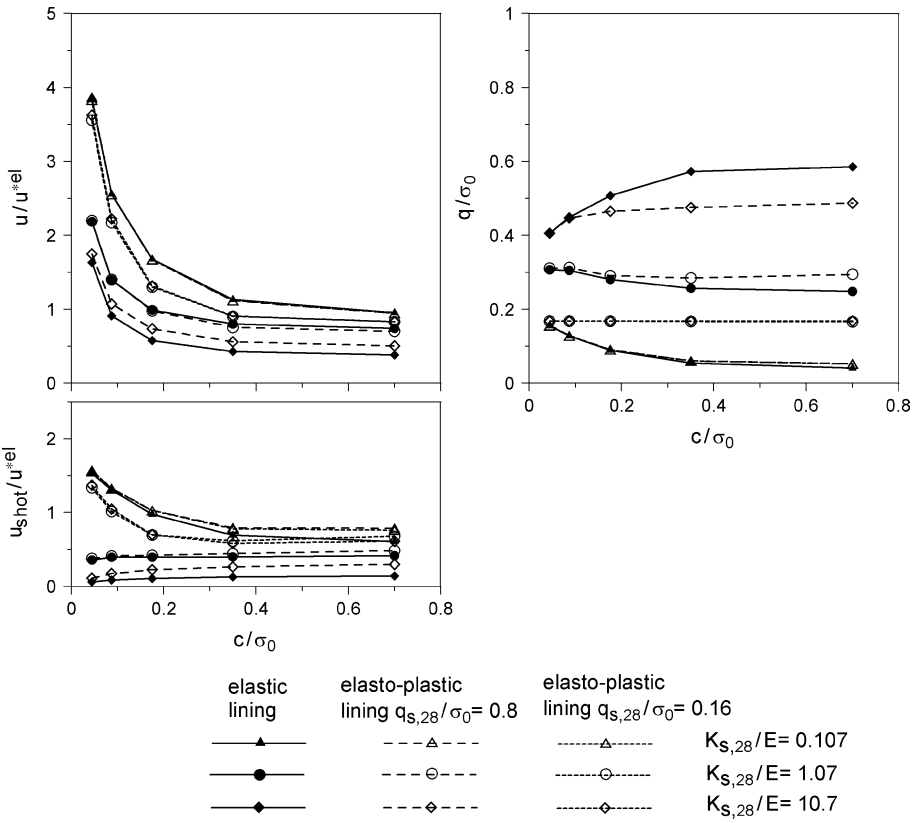

Fig. 14. Influence of the scaled lining strength $q_{s,28}/\sigma_o$ on the equilibrium load q, tunnel wall displacement u and shotcrete lining displacement u_{shot} ($v = 2\,m/d$, $\varphi = 20°$, $\psi = 0°$, $l = 1\,m$)

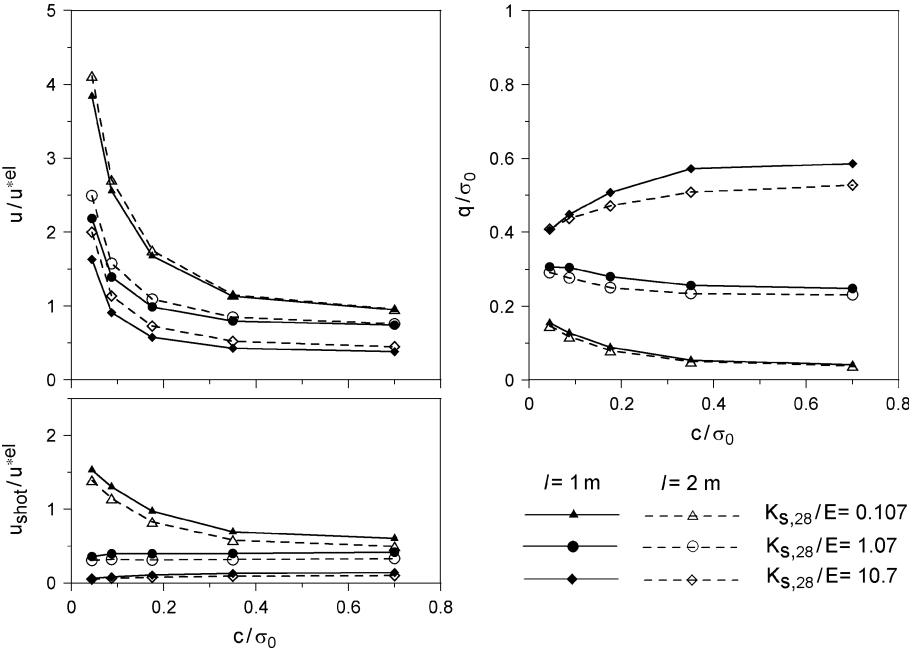

Fig. 15. Influence of the length l of the excavation step on the equilibrium load q, tunnel wall displacement u and shotcrete lining displacement u_{shot} (elastic lining, $\varphi = 20°$, $\psi = 0°$, $v = 2\,\text{m/d}$)

As already noted for the loadings, the displacements predicted by the CCM agree well with the numerical results (for $v = 0$) only for high-strength and low-stiffness ground properties; as ground cohesion and friction angle decrease, the CCM largely overestimates the ratio u/u^{*el}.

The deformation u_{shot} undergone by the shotcrete annulus (Fig. 10), closely related to the load q, is a key parameter in assessing the shotcrete cracking threshold.

The effect of ground strength (c/σ_o and φ) on the scaled displacement u_{shot}/u^{*el} is important only in the case of low relative stiffness K_s/E, particularly when the advance rate is high ($v = 8\,\text{m/d}$). It can be argued that, apart from the above mentioned case, the ground surrounding the shotcrete annulus generally undergoes an elastic unloading, due to the confinement action of the lining itself, so that the influence of the previous plastic deformations become negligible. Again, the ratio u_{shot}/u^{*el} is mainly affected by the relative stiffness K_s/E. Moreover, the increase in the advance rate produces a moderate but still significant increase in the ratio u_{shot}/u^{*el}, due to the assumed time-dependency of the shotcrete stiffness.

The CCM generally underestimates the displacement ratio u_{shot}/u^{*el}, particularly in the range of high relative stiffness.

In Fig. 11 the influence of the dilatancy angle ψ is analyzed, by comparing tunnel behavior in the cases of $\psi = 0°$ and $\psi = \varphi/2$. As expected, the dilatant behavior amplifies the tunnel convergence more when ground strength is lower, while the stress-strain state of the lining is only slightly affected.

A subset of numerical cases are devoted to investigating the influence of the plastic yielding of the shotcrete, according to Eq. (6). Figure 12 shows the time evolution of

the pressure on the lining calculated by assuming elastic or elasto-plastic behaviors of the shotcrete in two typical cases, characterized by different values of relative stiffness; for comparison, the time evolution of the yield pressure (defined as $q_s = \sigma_s \cdot e/a$) is represented as well. The impact of plastic yielding is relevant only in the case of a high value of the relative stiffness K_s/E.

To gain a better understanding, the scaled load q/σ_o has been plotted as a function of the face distance x in Fig. 13. Here, the step-wise loading of the shotcrete segments is clearly visible: because of the non-uniform stress along the shotcrete segment, plastic deformations develop within a short length of the shotcrete segment close to the face, during the earliest stages of the loading.

It is worth noting that the freshly applied shotcrete exhibits remarkable ductile properties (see Section 3.1), which allow for quite large deformations before cracking phenomena initiate.

A summary of the results obtained for elasto-plastic shotcrete behavior is presented in Fig. 14.

The key-role is played by the scaled yield load $q_{s,28}/\sigma_o$ and, once again, by the relative stiffness. Two typical values of $q_{s,28}/\sigma_o$ are considered: the lower value (0.16) represents the case of a very deep tunnel while the higher one (0.8) a more shallow tunnel. For a low ratio K_s/E, the results of the two cases coincide because the lining behaves elastically. For the intermediate value of K_s/E, the influence of the plastic behavior of the lining is remarkable only for the deep tunnel, where the pressure on the lining always equals the maximum yield load of the shotcrete annulus.

Only if a high relative stiffness is considered, the behavior of the more shallow tunnel is significantly influenced by the plastic deformation of the lining; the equilibrium pressure is noticeably lower than the value predicted for the elastic lining but still less than the maximum yield load. In fact the shotcrete annulus exhibits plastic deformation only at the very early loading steps, before the stationary conditions are attained (see also Figs. 12–13).

Finally the influence of the length of the excavation step is analyzed. The change in the ratio $l/2a$ (pull length/diameter) from $1/10$ to $1/5$ produces only a slight reduction in the average load and displacement of the shotcrete segment (Fig. 15), although the maximum load at the tip of the segment on the face-side increases considerably. This stress concentration effect increases markedly as the relative stiffness K_s/E increases, but it is almost smoothed down by averaging within the length l.

6. Back-Estimate of Stress Relief Factors

As mentioned in Section 2, conventional design methods for deep tunnels make use of the so-called stress relief factor λ to account for the displacement already developed at the time of lining installation. In the conventional CCM, the λ factor calculated by Eq. (4) depends only on the ground properties and on the face distance at the time the lining is placed.

In the following, a simple strategy for improving the accuracy of the conventional methods is presented. The proposed approach utilizes the results of 3D numerical models to back-calculate an equivalent λ factor, which accounts for the influence of

the lining-ground relative stiffness, the excavation rate and the shotcrete time-hardening process.

The back-calculation is performed in the (q, u) plane (Fig. 1) starting from the equilibrium pressure obtained in the 3D numerical analysis, indicated here as q_{eq}. Moving back along a conventional confinement curve, characterized by a constant slope, set equal to the stiffness of the shotcrete annulus at 28 days $K_{s,28}$, it is straightforward to determine the corresponding value of convergence at the time of lining installation u_0, and then the corresponding λ factor.

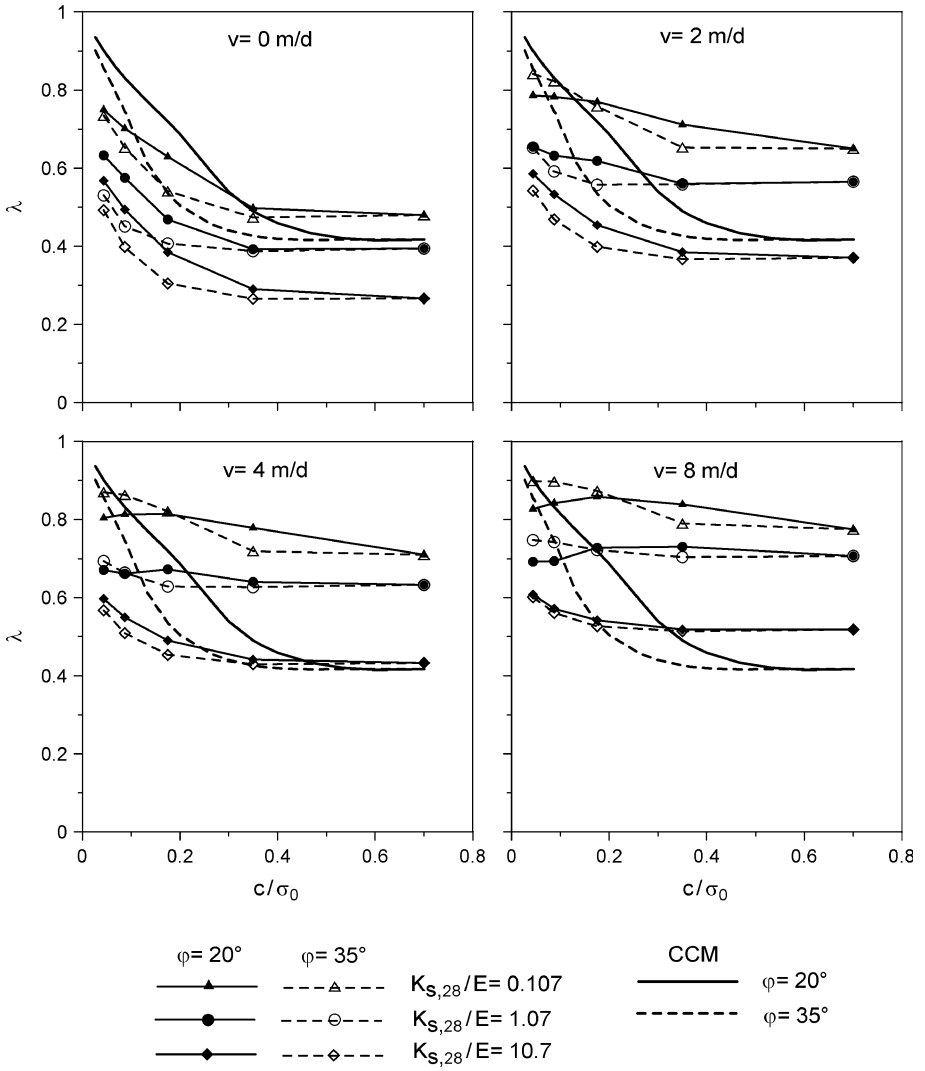

Fig. 16. Back-calculated stress release factors λ for different values of $K_{s,28}$, φ and v and comparison with the CCM results (elastic lining, $\psi = 0°$, $l = 1$ m)

Figure 16 shows the back-calculated λ factor for the full range of parameters $K_{s,28}/E$, c/σ_o, φ and v. The influence of the relative stiffness $K_{s,28}/E$ is always remarkable whatever the advance rate, while the influence of ground strength (c/σ_o and φ) is particularly remarkable when $v = 0$.

The λ factor appears to be as a decreasing function of cohesion until an almost horizontal threshold corresponding to the case of purely elastic behavior is reached. The influence of the advance rate increases in importance, the more the ground behaves elastically.

The λ factors obtained by the conventional CCM, calculated by assuming a distance x_o from the face at the time of lining installation equal to $0.5l$, are also represented in Fig. 16.

Large differences between the back-calculated λ and those obtained by the conventional CCM come from the observation of Fig. 16. In the case of elastic ground, the conventional CCM generally underestimates the λ factor, while in the case of low-strength elasto-plastic ground, it leads to a large overestimation. In the latter case the main discrepancy between the relaxation factors obtained by the CCM and the back-calculated λ is found for high relative stiffness, typical of poor rock mass conditions where support plays a key role for the stability of the excavation.

7. Example Applications

The proposed approach has been applied to some well documented case histories in order to validate the theoretical model and verify the consistency of the preliminary support design guidelines given in Section 6. Two cases have been analyzed: the first is a hydraulic tunnel (Pont Ventoux, Italy), which is now being excavated in a fractured hard-rock under high overburden, the second case is an experimental tunnel (Kielder, England) driven under a lower overburden in a thinly laminated soft-rock.

While most of the data concerning the excavation and support of the Pont Ventoux tunnel have been directly analyzed by the Authors, the behavior of the Kielder tunnel has been extensively studied in the geotechnical literature.

7.1 The Pont Ventoux Tunnel

The case study considers the behavior of one stretch of a 14 km long free-flow tunnel, which from the intake located at Pont Ventoux diverts the waters of the Dora Riparia river (Susa valley, Italy) to a compensation reservoir, where the pressure tunnel of the hydropower plant begins.

The tunnel crosses a quartzitic mica schist formation characterized by variable joint spacing and joint conditions ranging from ''good'' to ''very poor'', depending on the intersection of fault systems which typically have a clay filling of about 0.1 m.

Starting from the outlet side, a long stretch of the tunnel was initially excavated by an open TBM. At present the excavation is being completed by drill and blast with a horse shoe cross-section (equivalent radius 2.75 m). A more comprehensive description of the difficult geotechnical conditions faced during TBM advance can be found in Barla and Pelizza (2000).

The tunnel stretch to be examined herein (chainage 3000–3300 m) was excavated by blasting from the Pont Ventoux side with an advance rate of about 3 m/day, under

Table 3. Rock mass and tunnel parameters (Pont Ventoux example)

Rock mass		Tunnel excavation and support	
$\sigma_o = 9.35$ MPa	$\varphi = 33°$	$E_{s,28} = 24$ GPa	$a = 2.75$ m
$E = 5.3$ GPa	$c = 1.15$ MPa	$\nu_s = 0.3$	$l = 1$ m
$\nu = 0.25$	$\psi = 0°$	$e = 0.12$ m	v = 3 m/d
$h = 400$ m		$\sigma_{s,28} = 22$ MPa	

an average overburden of 400 m. On the basis of laboratory triaxial tests, the intact cores can be assigned a uniaxial strength $\sigma_{ci} = 70$ MPa and a Hoek's strength criterion with $m_i = 11$.

The fair-to-good quality of the rock mass (average joint spacing = 0.3 m, GSI = 50) within this stretch of tunnel has made it possible to use of a fiber-reinforced shotcrete ring as primary support, without the installation of a regular pattern of rock bolts. It is therefore easier to compare the observed behavior of the tunnel with the model prediction.

The rock mass parameters used in the numerical calculations (Table 3) have been evaluated from laboratory triaxial tests and rock mass classification by applying the standard procedure suggested in Hoek et al. (2002); a disturbance factor D = 0.7 has been assumed.

In Fig. 17 the convergence of the excavation profile (as a function of face distance x) predicted by the axisymmetric model is compared to the available set of measurements carried out in the monitoring sections between chainage 3000 and 3300. Figure 17 gives a clear picture of the typical scattering of actual displacement measurements even where the overall geotechnical conditions can be reasonably considered homogeneous; the ability of the proposed model to grasp the average behavior of the tunnel is however apparent.

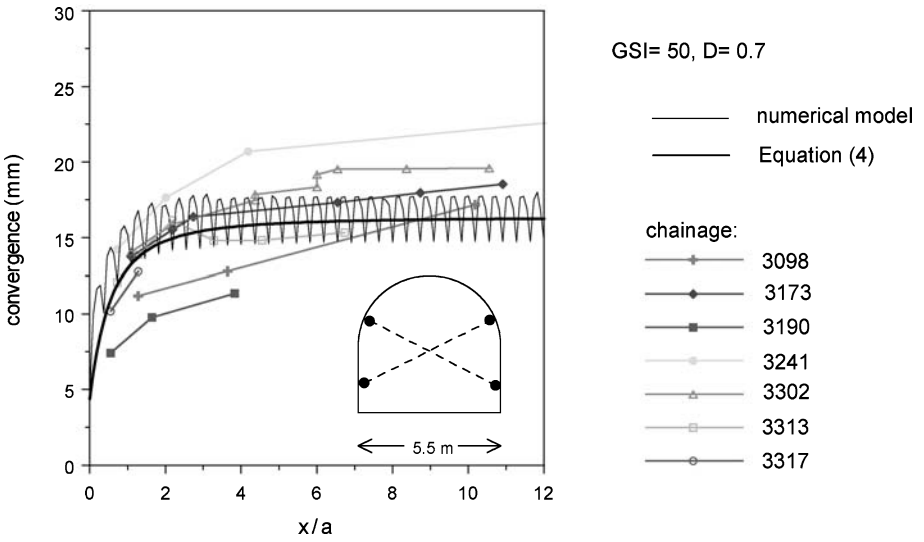

Fig. 17. Convergence profile predicted by the numerical model and convergence curves $C(x)$ measured by the monitoring sections (Pont Ventoux tunnel, chainages 3000–3300)

Table 4. Results obtained for the Pont Ventoux tunnel

	u/u^{*el}	u_{shot}/u^{*el}	q/σ_o	λ
Numerical model	1.35	0.67	0.074	0.78
Design charts	1.40	0.75	0.070	0.80

Note that in order for the measured convergence curves to be compared with each other and with the numerical model, it has been necessary to estimate the amount of convergence already developed in each of the monitoring sections prior to the beginning of the measurements, which usually started at a distance of 1–3 m from the face. This has been achieved by assuming relationship (4) as a shape function for the convergence curve $C(x)$ and hence estimating the section-specific u_∞ value on the basis of the first measurement of convergence increment.

Most of the monitoring sections exhibit a sizeable amount of time-dependent deformations as well, as detectable by convergence measurements that go on increasing even after the face-effect is exhausted (i.e. for $x > 2a$).

One more issue to be discussed is the consistency of the rough estimate of convergence and load, as obtained by interpolation on the design charts of Figs. 8 and 10, with the results of the purposely-developed numerical model, in which all the values of the parameters relevant to the specific case are introduced (see Table 4). The maximum deviation between the exact and approximated calculation is in the order of 10%: the use of the proposed design charts therefore seems to be acceptable at least as a preliminary design tool.

7.2 The Kielder Experimental Tunnel

This is a purely experimental tunnel (3.2 m diameter, 100 m depth) built in association with the main tunnel of the Kielder Water Scheme in a typical carboniferous shale called the Four Fathom Mudstone.

The Four Fathom mudstone is a highly fissile non-swelling shale with horizontal bedding planes every 25–35 mm and two sets of near vertical joints (average spacing 0.7 m). From the data reported in Hoek and Brown (1980), the rock mass may be classified with an RMR = 32.

A full assessment of the geotechnical parameters, based on laboratory tests as well as on the back-analysis of field measurements has been carried out by Ogawa and Lo (1987). The same set of data has been used for the present analysis, with minor simplifications due to the assumption herein of an ideal-plastic strength criterion (Table 5).

Table 5. Rock mass and tunnel parameters (Kielder experimental tunnel)

Rock mass		Tunnel excavation and support	
$\sigma_o = 2.56$ MPa	$\varphi = 25°$	$E_{s,28} = 28$ GPa	$a = 1.6$ m
$E = 5$ GPa	$c = 0.15$ MPa	$\nu_s = 0.3$	$l = 2$ m
$\nu = 0.25$	$\psi = 0°$	$e = 0.10$ m	v = 5 m/d
$h = 100$ m		$\sigma_{s,28} = 24$ MPa	

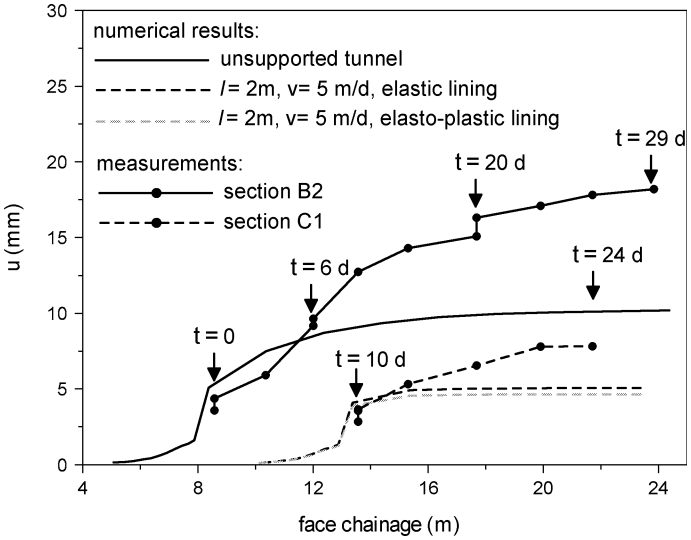

Fig. 18. Radial displacement vs face chainage measured at the tunnel crown in monitoring sections B2 and C1 (Kielder experimental tunnel) and numerical model predictions

The initial stage of its construction was completed in 1974; a 30 m extension was then excavated by drill and blast in 1977 to study the effect of increasing support delay on tunnel behavior in more detail. For this purpose a series of similar rings of shotcrete was placed in the extension at varying times after excavation had taken place; an unsupported length, where tunnel collapse was observed, is also included (Ward et al., 1983).

The 30 m long extension was advanced in 16 blasts; in each round, 2 m long as average, a multi-point rock extensometer was installed in the tunnel crown vertically upwards as soon as possible after spoil removal, close to the face (0.7 m distance).

Figure 18 shows the development of rock displacements at the tunnel crown as a function of face advance (after Ward et al., 1983). Only two monitoring sections will be analyzed herein: Section B, which was left initially unsupported, and Section C, where a shotcrete layer (minimum thickness 0.1 m) was placed up to the face 2.1 days after blasting. For this section, the age of the shotcrete at the time the adjoining face was advanced was equal to only 0.2 days, which corresponds to an average advance rate of 5 m/day. In the same Fig. 18, the prediction of crown displacements afforded by the numerical models with the data of Table 5 are also represented.

It is worthwhile noting that the excavation could not be advanced on a regular time-rate. In the numerical model an advance rate of 5 m/d was assumed in order to exactly match the effective mechanical properties of the shotcrete at the time of the first loading step, even if the advance rate slowed down in the next rounds.

The convergence developed before the beginning of extensometer readings has been assessed by applying relationship (4), as already done in the foregoing example, and by assuming $u_f = 1$ mm on the basis of available field observations (Hoek and Brown, 1980).

It is not surprising that for the unsupported section, the calculated displacements fit the experimental data only in the initial part, i.e. for a distance falling within the range of influence of the face, which in turn corresponds to a time-interval of 6–7 days after the face passes through the monitoring section. In fact it should be recalled that the strength parameters given by Ogawa and Lo (1987) are only representative of rock conditions immediately after excavation, because "when exposed, the mudstone is prone to rapid deterioration and quickly forms a soil-like mass". It can therefore be argued that the mudstone exhibits a strong time-decrease of its cohesive strength possibly associated with creep deformation, as a subsidiary phenomenon.

The convergence of the supported section is effectively controlled by the shotcrete, which acts by applying a confining pressure as well as by sealing the tunnel wall, thus avoiding the progressive deterioration of the mudstone.

The behavior of the Kielder tunnel was markedly affected by the anisotropy of the rock mass, mainly due to the horizontal bedding planes, which first enforced a "square" more than a "circular" excavation profile, and thereafter caused a vertical deformation at the crown larger than the horizontal deformation at the sidewalls, also associated in some cases with loosening of the roof strata and local flexural behavior at the crown of the shotcrete arch.

Despite the crude idealizations introduced in the model, the development of convergence in the supported section is reasonably well predicted by the model, even though the stabilized convergence is slightly underestimated as well as the time required to reach such "asymptotic" conditions.

The ability of the model to estimate the overall response of the supported section is confirmed by Fig. 19, where the development in time of circumferential strains within the shotcrete ring is shown. The predicted final deformation u_{shot}/a compares well with the average strains measured by the 12 vibrating-wire gouges (6 near the rock surface and 6 near the inner face) positioned in each quadrant of the tunnel (Ward et al., 1983).

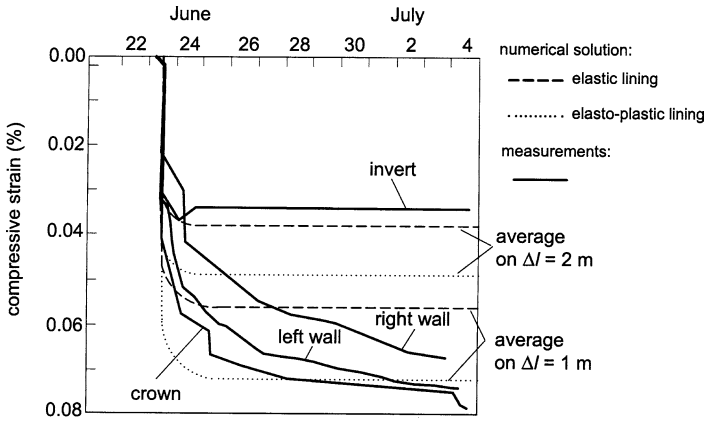

Fig. 19. Time development of circumferential strains measured within the shotcrete ring (Kielder experimental tunnel, section C1) and numerical model predictions for elastic and elasto-plastic shotcrete behavior: average strain in the whole ring ($\Delta l = 2$ m) and in half the segment on the face side ($\Delta l = 1$ m)

8. Conclusions and Critical Remarks

The construction process of a shotcrete-supported tunnel has been modeled step-by-step, limiting the number of time-dependent parameters to only two (i.e., Young's modulus and uniaxial strength of the shotcrete), with time-increases being controlled by the rate of excavation and support installation.

Despite the crude idealization of the mechanical behavior as well as of the construction process and geometry, the model gives a rational framework for support design, which represents a step forward from the simplistic assumption of a "reduced" shotcrete modulus and represents a compromise between rough design methods and detailed numerical modeling.

The results of the parametric analyses have been used to set up approximate design guidelines, focusing on the average behavior of the shotcrete ring placed in a single round.

The main lessons learnt from the analyses are:

- an increasing excavation rate implies a reduction in the load as well as a smoothing down of the stress-strain profile within the single shotcrete ring;
- the relative stiffness between the ground and the support system is the factor with the strongest influence on equilibrium loads;
- ground yielding affects more the pre-convergence of the tunnel wall than the loading conditions and convergence after support installation;
- the influence of the plastic behavior of the shotcrete is remarkable only for very deep tunnels, where the final loads often reach the maximum yield load of the shotcrete ring.

The application of the proposed approach to two real cases has shown that predicted short-term displacements of the tunnel wall as well as average strain of the shotcrete ring match the monitoring results reasonably well, even if the measured deformations exhibit a more gradual time-increase and higher stationary values due to time-dependent creep and damage of the rock mass. Such phenomena can be particularly important for deep tunnels in poor ground conditions, where the creep properties of the green shotcrete also play a crucial role by considerably enhancing the ductile behavior of the support, resulting in the capacity to tolerate larger deformations at yield-loading conditions.

Full exploitation of the support strength, which would be unacceptable for the serviceability design of permanent structures, is not uncommon for the shotcrete shell used as primary support in squeezing ground conditions. In this case special devices, such as pre-formed slots and collapsible joints may also be arranged to avoid pervasive cracking phenomena which would impair the structural integrity of the shotcrete shell (Schubert, 1996).

In many cases it was also observed that the simultaneous creep deformations of both ground and concrete lead to significantly larger long-term convergence even though the severity of the state of stress within the support is not significantly increased (Pöttler, 1990). A close examination of the problem requires the application of elasto-visco-plastic material models and a careful monitoring of the long-term tunnel behavior (Boldini et al., 2003).

Discrepancies between measured and calculated behavior may also stem from the following reasons:

– a strong but unavoidable idealization of the irregular tunnel section profile and even more of the variable thickness of the shotcrete layer;
– the assumption that excavation and shotcreting operations progress regularly (i.e. constant advance rate and pull length), while, in practice variable times, unforeseen stops and local changes in geometry may occur.

In conclusion, the proposed guidelines for support design and λ-factor assessment can be a valuable predictive tool in most routine tunneling projects and can at least allow for a preliminary screening to identify particularly demanding situations which could require more sophisticated analyses.

List of Symbols

a	tunnel radius
c	cohesion of the ground mass
C	convergence of the tunnel (diameter reduction)
e	thickness of the shotcrete annulus
E	Young's modulus of the ground mass
E_s	Young's modulus of the shotcrete
$E_{s,28}$	Young's modulus of the shotcrete at 28 days
h	depth of the tunnel
K_s	stiffness of the shotcrete annulus
$K_{s,28}$	stiffness of the shotcrete annulus at 28 days
l	length excavated per round
N_x	axial force in the longitudinal direction
N_θ	axial force in the circumferential direction
$N_{\theta m}$	average value of N_θ within a segment
M_x	bending moment in the longitudinal direction
M_θ	bending moment in the circumferential direction
p_i	internal pressure applied at the tunnel wall
q	pressure on the extrados of the lining
q_{eq}	equilibrium pressure on the extrados of the lining (CCM)
q_s	yield load (pressure) of the shotcrete annulus
$q_{s,28}$	yield load (pressure) of the shotcrete annulus at 28 days
R_p	plastic radius
t	time
u	radial displacement of the tunnel wall
u_f	radial displacement of the tunnel wall at the face
u_0	radial displacement of the tunnel wall at the time of lining installation
u_{shot}	radial displacement of the shotcrete lining
u^{*el}	radial displacement of the unlined tunnel at great distance from the face (elastic material)
u_∞	final radial displacement of the unlined tunnel at great distance from the face
v	tunnel excavation rate
x	distance from the tunnel face
x_0	distance between the tunnel face and the section where the lining is installed
λ	stress release factor
λ_{CC}	stress release factor obtained by the conventional CC method
ν	Poisson's ratio of the ground mass
ν_s	Poisson's ratio of the shotcrete

σ_o isotropic in situ stress
σ_s uniaxial compressive strength of the shotcrete
$\sigma_{s,28}$ uniaxial compressive strength of the shotcrete at 28 days
φ friction angle of the ground mass
ψ dilatancy angle of the ground mass

References

A.F.T.E.S. (1983): Recommandations sur l'emploi de la méthode convergence-confinement, 206–222.

Anagnostou, G., Kovari, K. (1993): Significant parameters in elastoplastic analysis of underground openings. J. Geotech. Eng. (ASCE) 119(3), 401–419.

Barla, G., Pelizza, S. (2000): TBM tunnelling in difficult ground conditions. In: Barla, G. (ed.) VIII Ciclo di Conferenze di Meccanica ed Ingegneria delle Rocce (MIR 2000), Torino, 329–354.

Bernaud, D., Rousset, G. (1992): La nouvelle méthode implicite pour l'étude du dimensionnement des tunnels. Rev. Franç. Géotech. 60, 5–26.

Bernaud, D., Rousset, G. (1996): Short communication – The new implicit method for tunnel analysis. Int. J. Numer. Anal. Meth. Geomech. 20, 673–690.

Boldini, D., Lackner, R., Mang, H. A. (2003): Elucidation of ground-lining interaction in NATM tunneling accounting for chemo-mechanical couplings in shotcrete behavior. In: Viggiani, C. (ed.) Work. Constitutive Modelling and Analysis of Boundary Value Problems in Geotechnical Engineering, Napoli, 461–487.

Brown, E. T., Bray, J. W., Ladanyi, B., Hoek, E. (1983): Ground response curves for rock tunnels. J. Geotech. Eng. (ASCE) 109(1), 15–39.

Carranza-Torres, C. (2003): Dimensionless graphical representation of the exact elasto-plastic solution of a circular tunnel in a Mohr-Coulomb material subject to uniform far-field stresses. Rock Mech. Rock Engng. 36(3), 237–253.

Chang, Y. (1994): Tunnel support with shotcrete in weak rock – A rock mechanics study. Ph.D. Thesis, Division of Soil and Rock Mechanics, Royal Institute of Technology, Stockholm, Sweden.

Corbetta, F., Bernaud, D., Nguyen Minh, D. (1991): Contribution à la méthode convergence-confinement par le principe de la similitude. Rev. Franç. Géotech. 54, 5–11.

Cosciotti, L., Lembo-Fazio, A., Boldini, D., Graziani, A. (2001): Simplified behavior models of tunnel faces supported by shotcrete and bolts. In: Adachi, T., Tateyama, K., Kimura, M. (eds.), Int. Conf. Conference on Modern Tunneling Science and Technology (IS-Kyoto 2001), Kyoto, Japan, vol. 1, 407–412.

Einstein, M., Schwartz, C. (1979): Simplified analysis for tunnel support. J. Geotech. Geoenviron. Eng. (ASCE) 105, 499–518.

Hoek, E. (2001): Big tunnels in bad rock. J. Geotech. Geoenviron. Eng. (ASCE) 127(9), 726–740.

Hoek, E., Brown, E. T. (1980): Underground excavations in rock. IMM, London.

Hoek, E., Carranza-Torres, C., Corkum, B. (2002). Hoek-Brown failure criterium. – 2002 Edition. In: Proc. 5th NARMS-TAC, Toronto.

Itasca (2000): FLAC 4.0 User's guide. Itasca Consulting Group, Minneapolis.

Kielbassa, S., Duddeck, H. (1991): Stress-strain fields at the tunnelling face – Three-dimensional analysis for two-dimensional technical approach. Rock Mech. Rock Engng. 24(3), 115–132.

Lombardi, G. (1973): Dimensioning of tunnel linings with regard to constructional procedure. Tunnels Tunneling July, 340–351.

Lunardi, P. (2000): Design & constructing tunnels – ADECO-RS approach. Tunnels Tunnelling Int., Spec. Suppl., May 2000, 1–30.

Nguyen-Minh, D., Corbetta, F. (1991): Nouvelles méthodes de calcul des tunnels rêvetus incluant l'effet du front de taille. In: Wittke, W. (ed.) 7th Int. Symp. Rock Mechanics, Aachen, Germany, 2, 1335–1338.

Ogawa, T., Lo, K. Y. (1987): Effects of dilatancy and yield criteria on displacements around tunnels. Can. Geotech. J. 24, 100–113.

Oreste, P. P. (2003): A procedure for determining the reaction curve of shotcrete lining considering transient conditions. Rock Mech. Rock Engng. 36(3), 209–236.

Panet, M., Guellec, P. (1974): Contribution à l'étude du soutènement derrière le front de taille. In: Proc. 3rd Congr. ISRM, Denver, 2, part B, 1130–1134.

Panet, M., Guenot, A. (1982): Analysis of convergence behind the face of a tunnel. Tunneling 82, Brighton, United Kingdom, 197–204.

Pöttler, R. (1990): Time-dependent rock-shotcrete interaction. A numerical shortcut. Computers Geotechnics 9, 149–169.

Ribacchi, R., Riccioni, R. (1977): Stato di sforzo e deformazione intorno ad una galleria circolare. Gallerie e Grandi Opere in Sotterraneo 4, 7–17.

Schubert, W. (1996): Dealing with squeezing conditions in Alpine tunnels. Rock Mech. Rock Engng. 29(3), 145–153.

Sezaki, M., Kibe, T., Ichikawa, Y., Kawamoto, T. (1989): An experimental study on the mechanical properties of shotcrete. J. Soc. Mater. Sci. 38, 1336–1340.

Stille, H., Holmberg, M., Nord, G. (1989): Support of weak rock with grouted bolts and shotcrete. Int. J. Rock Mech. Min. Sci. Geomech. Abstr. 26(1), 99–113.

Vogt, C., Bonnier, P., Vermeer, P. A. (1998): Analyses of NATM-tunnels with 2D and 3D Finite Element Method. In: NUMGE98 Application of numerical methods to geotechnical problems, Udine, CISM, 211–219.

Ward, W. H., Tedd, P., Berry, N. S. M. (1983): The Kielder experimental tunnel: final results. Géotechnique 33(3), 275–291.

Wong, R. C. K., Kaiser, P. K. (1991): Performance assessment of tunnels in cohesionless soils. J. Geotech. Eng. (ASCE) 117(12), 1880–1901.

Authors' address: Dr. Alessandro Graziani, Dr. Daniela Boldini, Prof. Renato Ribacchi, Universitá di Roma "La Sapienza", Dipartimento di Ingegneria Strutturale e Geotecnica, Via Monte d'Oro 28, 00186 Rome, Italy; e-mail: alessandro.graziani@uniroma1.it, daniela.boldini@uniroma1.it, renato.ribacchi@uniroma1.it